



**HAL**  
open science

## Evidence of the Current Collector Effect: Study of the SOFC Cathode Material $\text{Ca}_3\text{Co}_4\text{O}_9+\delta$

A. Rolle, V. Thoréton, Patrick Rozier, E. Capoen, O. Mentré, B. Boukamp, S. Daviero-Minaud

► **To cite this version:**

A. Rolle, V. Thoréton, Patrick Rozier, E. Capoen, O. Mentré, et al.. Evidence of the Current Collector Effect: Study of the SOFC Cathode Material  $\text{Ca}_3\text{Co}_4\text{O}_9+\delta$ . Fuel Cells, 2012, 12 (2), pp.288-301. 10.1002/face.201100084 . hal-02069357

**HAL Id: hal-02069357**

**<https://hal.science/hal-02069357>**

Submitted on 22 Oct 2019

**HAL** is a multi-disciplinary open access archive for the deposit and dissemination of scientific research documents, whether they are published or not. The documents may come from teaching and research institutions in France or abroad, or from public or private research centers.

L'archive ouverte pluridisciplinaire **HAL**, est destinée au dépôt et à la diffusion de documents scientifiques de niveau recherche, publiés ou non, émanant des établissements d'enseignement et de recherche français ou étrangers, des laboratoires publics ou privés.




## Open Archive Toulouse Archive Ouverte (OATAO)

OATAO is an open access repository that collects the work of Toulouse researchers and makes it freely available over the web where possible

This is an author's version published in: <http://oatao.univ-toulouse.fr/24433>

**Official URL:** <https://doi.org/10.1002/fuce.201100084>

**To cite this version:**

Rolle, Aurélie and Thoréton, Vincent and Rozier, Patrick  and Capoen, Edouard and Mentré, Olivier and Boukamp, Bernard and Daviero-Minaud, Sylvie *Evidence of the Current Collector Effect: Study of the SOFC Cathode Material  $\text{Ca}_3\text{Co}_4\text{O}_{9+\delta}$* . (2012) *Fuel Cells*, 12 (2). 288-301. ISSN 1615-6846

Any correspondence concerning this service should be sent to the repository administrator: [tech-oatao@listes-diff.inp-toulouse.fr](mailto:tech-oatao@listes-diff.inp-toulouse.fr)

# Evidence of the Current Collector Effect: Study of the SOFC Cathode Material $\text{Ca}_3\text{Co}_4\text{O}_{9+\delta}$ ▲

A. Rolle<sup>1\*</sup>, V. Thoréton<sup>1</sup>, P. Rozier<sup>2</sup>, E. Capoen<sup>1</sup>, O. Mentré<sup>1</sup>, B. Boukamp<sup>3</sup>,  
S. Daviero-Minaud<sup>1</sup>

<sup>1</sup> Univ. Lille Nord de France F-59000 Lille, CNRS UMR 8181–Unité de Catalyse et de Chimie du Solide–UCCS, ENSC, USTL bat C7 avenue Dimitri Mendeleïev, BP 90 108, F-59652 Villeneuve d’Ascq cedex, France

<sup>2</sup> Centre d’Elaboration de Matériaux et d’Etudes Structurales, UPR CNRS 8011, 29, rue Jeanne Marvig, BP 94 347, 31 055 Toulouse Cedex 4, France

<sup>3</sup> Faculty of Science & Technology & MESA<sup>+</sup>, Institute for Nanotechnology, University of Twente, P. O. Box 217, 7500 AE Enschede, The Netherlands

## Abstract

In the study of the performance of solid oxide fuel cell (SOFC) electrodes, the possible influence of the applied current collector is often not mentioned or recognized. In this article, as part of an optimization study of the potentially attractive  $\text{Ca}_3\text{Co}_4\text{O}_{9+\delta}$  cathode material (Ca349), special attention is paid to the choice of current collector. The influence of both gold and platinum paste or grid current collectors on pure and composite (Ca349 + 30 wt.% Gd-doped ceria) is studied, using electrochemical impedance spectroscopy (EIS). Although, platinum is catalytically active in the oxygen reduction reaction and then is often considered as current collector for SOFC cathodes, in combination with Ca349 cathodes, additional low frequency dispersion is observed, leading to a larger polarization resistance than

found in the case of gold current collectors. A subsequent experiment revealed that Pt reacts with Ca349, forming undesirable phases:  $\text{CaPt}_2\text{O}_4$ ,  $\text{Ca}_4\text{PtO}_6$ ,  $\text{Ca}_3\text{Co}_2\text{O}_6$ , and  $\text{Co}_3\text{O}_4$ . The impedance spectra were analyzed with ZView 3.3a and with EqCwin v1.2. One series equivalent circuit was deduced using ZView, whereas, two possible equivalent circuits (series and nested), leading to the same quality of fits, were evidenced in EqCwin. The circuits are closely related to interactions of the current collector and layer thickness effects of the cathodes.

**Keywords:**  $\text{Ca}_3\text{Co}_4\text{O}_{9+\delta}$ , Cathode, Current Collection, Electrochemical Impedance Spectroscopy, Screen Printing, Solid Oxide Fuel Cell

## 1 Introduction

In a solid oxide fuel cell (SOFC), the fundamental part of the cathode model is the oxygen reduction pathway. The mechanisms involved at the cathode at the triple phase boundary, where the oxygen reduction reaction occurs, are quite complex and are often modeled using multi-step mechanisms. They imply interactions, which can take place on the surface, but also in the whole thickness of the cathode layer. The steps to consider are oxygen diffusion, oxygen adsorp-

tion/dissociation, charge transfer, and diffusion of ionic species [1]. They involve specific requirements for the considered materials in terms of microstructure, porosity, electrocatalytic properties, electronic/oxide ion conduction, and electrochemical properties. The cathode composition and morphology plays the main role. But one must keep in mind that the current collector can also interfere with the oxygen reduction reaction, especially if platinum is used. Indeed, its excellent catalytic properties toward this reaction justified its use as cathode in the first SOFCs developments [1–3].

▲ Paper presented at the “Fundamentals and Developments of Fuel Cells – Conference 2011”, January 19–21, 2011, Grenoble, France.

[\*] Corresponding author, aurelie.rolle@ensc-lille.fr

Within the framework of the study of cathodes for SOFCs, electrochemical impedance spectroscopy (EIS) is a method of choice to describe the electrochemical properties. However, drastic effects can be evidenced in the cathode electrochemical response according to the measurement conditions and more precisely the collector choice. In many studies using EIS to characterize the cathode properties, either the choice of current collector is not justified, or the type of current collector is not always specified. Generally platinum paste is used as current collector in the characterization of SOFCs' cathodes. We have recently pointed out as part of an optimization study of  $\text{Ca}_3\text{Co}_4\text{O}_{9+\delta}$  (Ca349, a potential cathode material [4, 5]), that particular attention should be paid on the choice of the current collector.

$\text{Ca}_3\text{Co}_4\text{O}_{9+\delta}$ , a thermoelectric material, is expected to have two-dimensional ionic conduction due to oxygen vacancies associated with the mixed valence of cobalt in 2D-rock salt subunits. It is also a good electronic conductor ( $\sigma = 100 \text{ S cm}^{-1}$  at  $700^\circ\text{C}$ ). It shows no reactivity with the gadolinium doped ceria standard electrolyte (CGO) and possesses a thermal expansion coefficient of  $9\text{--}10 \times 10^{-6} \text{ K}^{-1}$ , which makes it compatible with CGO [2].

In the article, all the abbreviations considered, the cells characteristics and the equivalent circuit symbols are provided in the Supplementary Data Section (S1, S2, S3). In Figure 1, the recently published results on Ca349 are summarized [4, 5]. The same description of samples as in ref. [5] will be used in this paper. The sample designations are described in more details in the Supplementary Data Section (S2). From these results, one trend has been observed: the polarization resistance is lower for Ca349/CGO composites than for the single-phase electrodes. Moreover, the lowest polarization resistance is obtained for the thicker layers. The lowest polarization resistance is currently reported in ref. [4] for the 70 wt.% Ca349–30 wt.% CGO composite cathode: approximately  $1 \Omega \text{ cm}^{-2}$  at  $700^\circ\text{C}$  measured on thick electrolyte support.

From the impedance diagrams presented in Figure 1, it is obvious that the use of platinum as current collector raises the question of a possible current collector effect.

With the aim to highlight the importance of the choice and on the effect of the current collector, this article focuses on the influence of several current collectors (gold grid, gold paste, platinum grid, and platinum paste) on the electrochemical response of the Ca349 cathodes. The impedance data has been analyzed with ZView 3.3a [6] and with EqCwin v1.2 (Windows version of Equivalent Circuit [7–9]), in which more detailed equivalent circuit models have been extracted.

## 2 Experimental

The synthesis of the Ca349 powder, the Ca349-based inks and the preparation of the pellets for the microstructural and electrochemical characterizations were performed as presented in ref. [5]. Cathode layers were screen-printed using a DEK 248 screen-printer. Depending on the type of sample/current collector assembly thermal treatments at  $700$ ,  $800$ , or  $900^\circ\text{C}$  were applied. More information on each cell is provided in the Table S2 given in the Supplementary Data Section. For current collector deposition, Au paste (Ferro couleurs, France SA), mixed with DH 43 (dmc<sup>2</sup> Limoges, France) was deposited by hand painting on the cell, followed by a thermal treatment at  $650^\circ\text{C}$  in order to decompose the organic part. The Pt paste (dmc<sup>2</sup> Limoges) was deposited similarly and treated at  $800^\circ\text{C}$ . EDS analysis has revealed the purity of the gold and platinum paste.

Microstructural characterizations were performed by scanning electron microscopy using a Hitachi S3400N SEM. X-ray diffraction was performed on powders and on deposited layers using a D8 Advance A25 Bruker with a Position Sensitive Detector Lynxeye or using a D8 Bruker AXS diffractometer ( $\text{CuK}\alpha = 1.54 \text{ \AA}$ ). In order to determine the oxygen mobility in Ca349, permeation measurements were carried out, using the same protocol as described in ref. [10], on

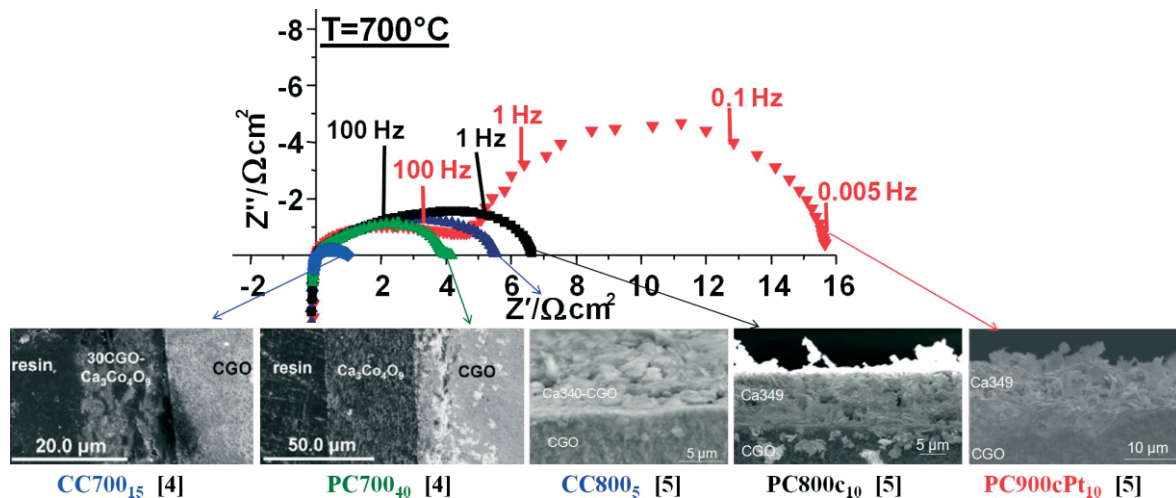


Fig. 1 Recently published data on Ca349 [4, 5].

dense pellets (97%) obtained by spark plasma sintering (SPS), performed in the PNF2 Platform ( $T_{\max} = 850\text{ °C}$  and  $P_{\max} = 50\text{ MPa}$ , densification starting at  $600\text{ °C}$  until  $850\text{ °C}$ ) (Toulouse, France).

Pellets have been checked by XRD. Impedance measurements were performed on symmetrical cells, cathode/electrolyte/cathode, using a SI 1260 Solartron FRA, during a heating-cooling sequence. An optimized signal amplitude of  $50\text{ mV}$  (pure Ca349) and  $70\text{ mV}$  (composite Ca349) were imposed, with respect to the linearity of the electrical response. Four types of current collectors were applied: gold grid, platinum grid, gold paste, and platinum paste. The data collection procedure was identical to the one reported in ref. [5]. At each temperature, the thermal and time stability were checked. The data were collected when the change in the polarization resistance was less than 5%. After a temperature change, measurements were performed as function of time. It was found that stability is reached within 2 h after each temperature change. The impedance data were analyzed using two different software packages: ZView 3.3a [6] and Equivalent Circuit 1.2. (Windows version EqCwin) [7–9]. For use of the latter programme, the stability and validity of the considered data was checked using the Kramers–Kronig (KK) test for Windows, version 1.01 [11, 12].

## 3 Results and Discussion

### 3.1 Ionic Conduction Properties

Ca349 is known for its good electrical conductivity property, which is reported to be higher than  $100\text{ S cm}^{-1}$  over the  $20\text{--}800\text{ °C}$  temperature range [4, 13]. However, the ionic conduction of this phase has never been checked before. For that purpose, permeation measurements were performed on  $0.5\text{ mm}$  thick and  $15\text{ mm}$  diameter SPS-dense pellets (relative density  $>97\%$ ) of the pure Ca349 material. Both faces of the pellets were polished with up to 2,400 grid and the experiments were carried out between  $580$  and  $650\text{ °C}$ . The oxygen flux is deduced from the  $\Delta p\text{O}_2$  variation at the permeate side. The oxygen permeation measurements revealed a significant oxygen flux even at low temperatures ( $0.0014\text{ }\mu\text{mol cm}^{-2}\text{ s}^{-1}$  at  $600\text{ °C}$ ), which unquestionably proves the existence of oxygen-ion migration (Table 1). For information, the oxygen fluxes reported for  $\text{La}_{0.6}\text{Sr}_{0.4}\text{Co}_{0.8}\text{Fe}_{0.2}\text{O}_{3-d}$  (LSCF) in the literature [14] are about  $0.00562\text{ }\mu\text{mol cm}^{-2}\text{ s}^{-1}$  at  $850\text{ °C}$ , but one can notice, that the membrane thickness,  $p\text{O}_2$  gradients,

and temperature range are different, making a direct comparison difficult. Nevertheless the flux measured for Ca349 is about the same order, but measured at significantly lower temperatures. However, after the permeation measurements, a surfacial passivation of Ca349 into CaO and CoO, was observed due to the long-exposure time of the pellet under Ar atmosphere at  $700\text{ °C}$ . This experiment confirms Ca349 as a mixed oxide ion and electronic conductor and shows its potentiality as cathode material in SOFC applications.

### 3.2 Current Collector Effect

#### 3.2.1 Gold Paste Versus Gold Grid

The same composite sample CC800<sub>20</sub> characterized in ref. [5] with gold grid only (CC800<sub>20</sub>) was also studied here with gold paste (CC800Au<sub>20</sub>) as current collector. The comparison between these two kinds of current collectors revealed that the electrochemical properties are the same, independent of the type of gold current collector. For example, the comparison of the impedance spectra recorded at  $700\text{ °C}$  is shown in Figure 2(a). A random shift of the series resistance is observed on the impedance spectra, reported Figure 2, which might be due to the global measuring set-up.

For this  $20\text{ }\mu\text{m}$  thick cathode layer, polarization resistances of  $1.39$  and  $1.41\text{ }\Omega\text{ cm}^2$  were obtained for the gold grid and the gold paste, respectively. The cross-section of the cell after EIS measurements is presented in Figure 3(a). The gold layer is about  $5\text{ }\mu\text{m}$  thick. After the EIS measurements no additional phase could be observed in the X-ray diffraction pattern [Figure 4(a)]. The reactivity test between Ca349 and Au at  $700\text{ °C}$  for  $72\text{ h}$  also revealed no interaction between these two phases, as can be noticed in the X-ray diffraction pattern of Figure 4(b). The impedance plots consist of a single depressed semicircle which does not change noticeably with time [Figure S4 in Supplementary Data Section]. From these results, it can be inferred that the impedance response represents the properties of Ca349 only.

#### 3.2.2 Platinum Paste Versus Gold Grid

A comparison of the electrochemical properties of identical composite CC800<sub>5</sub> cathodes with either platinum paste or gold grid as current collector is presented in Figure 2(b). These results have been reproduced from ref. [5]. Activation energies determined for the case of gold grid and platinum paste current collectors ( $1.15$  and  $1.52\text{ eV}$ , respectively), reveal that, when platinum paste is used as current collector, the cathode behavior is more complex and the ASR values are less favorable [5]. Special attention is paid to the impedance properties at  $700\text{ °C}$ . At this temperature, polarization resistances of about  $5.6$  and  $12.9\text{ }\Omega\text{ cm}^2$  are obtained, respectively, for gold grid and platinum paste used as current collector [5] with the same sample. Even if the platinum layer is quite thin [about less than  $1\text{ }\mu\text{m}$ , Figure 3(b)], a clear growing contribution is observable in the impedance plot at low frequency, as compared to the gold grid collector case. This

Table 1 Oxygen permeation measurements: comparison of Ca349 and LSCF.

Membrane	Ca <sub>3</sub> Co <sub>4</sub> O <sub>9+d</sub> (Ca349)	La <sub>0.6</sub> Sr <sub>0.4</sub> Co <sub>0.8</sub> Fe <sub>0.2</sub> O <sub>3</sub> (LSCF) [13]
Temperature / °C	600–700	850–1000
$J(\text{O}_2) / \mu\text{mol cm}^{-2}\text{ s}^{-1}$	0.0014–0.0020	0.00562–0.0316
Thickness / mm	0.50	0.55–0.98
$p'\text{O}_2 / \text{atm}$	1.00	0.21
	$3 \times 10^{-6}$	$1 \times 10^{-3}$

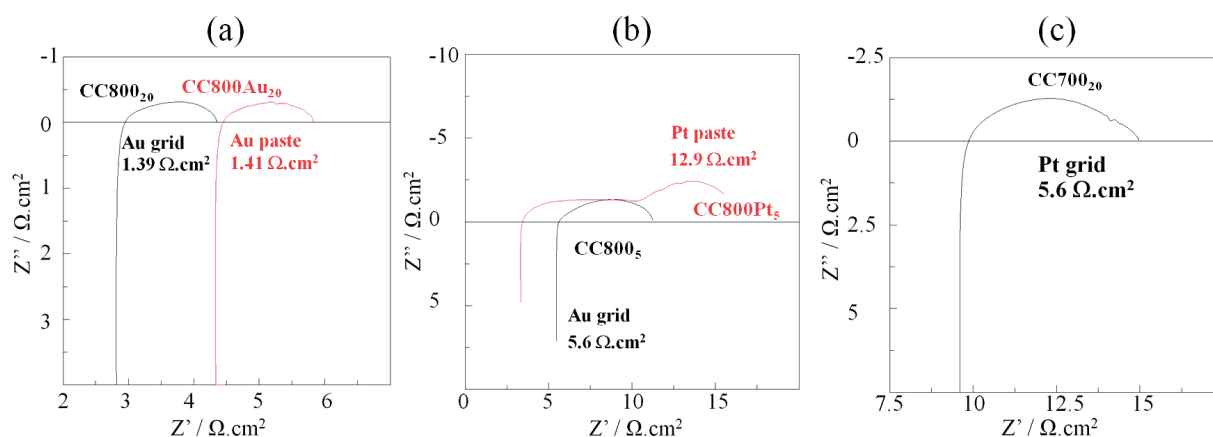


Fig. 2 Effect of the current collector on the electrochemical property: (a) gold paste-gold grid, (b) platinum paste-gold grid, and (c) platinum grid. Data are reported at 700 °C.

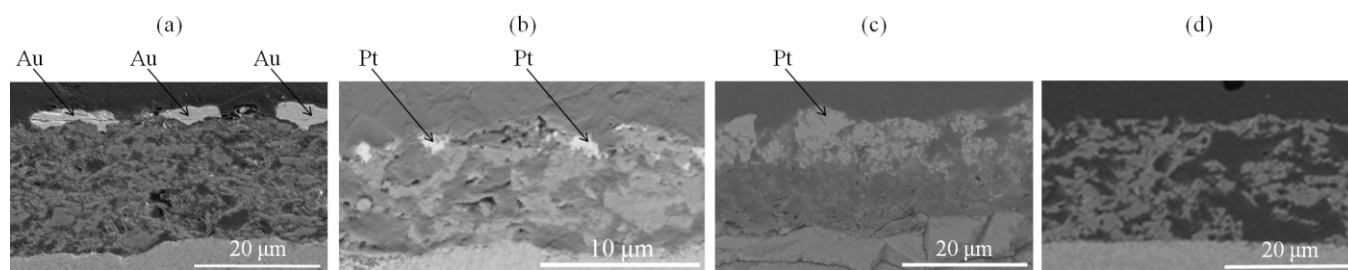


Fig. 3 SEM cross-section of (a) CC800Au<sub>20</sub>, (b) CC800Pt<sub>5</sub>, (c) CC900Pt<sub>10</sub>, and (d) CC700<sub>20</sub> after EIS characterization.

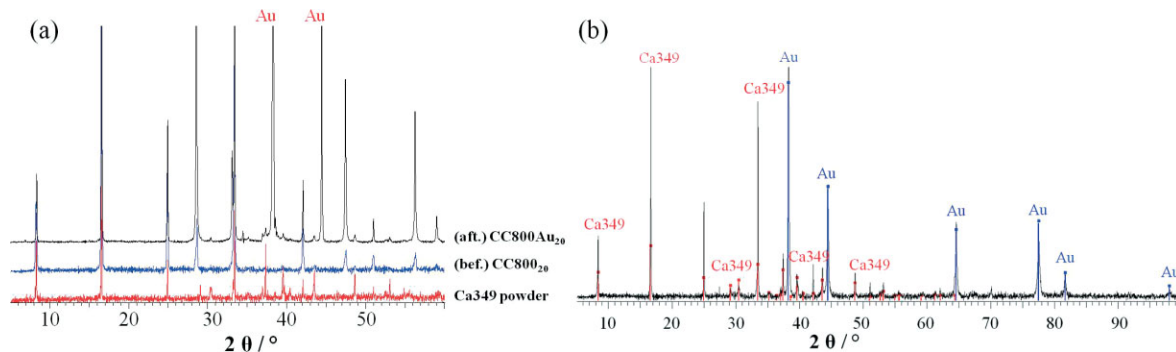


Fig. 4 (a) Comparison of the X-ray diffractograms of Ca349 powder, CC800<sub>20</sub>, and CC800Au<sub>20</sub> before gold painting (bef.) and after EIS measurements (aft.). (b) Reactivity test of Ca349 and gold at 700 °C for 72 h.

growing contribution is observed in the impedance plot of all the samples (pure as well as composite ones) measured with a Pt-paste current collector, independently of the platinum thickness [5]. X-ray diffraction was performed on the CC800<sub>5</sub> pellets after EIS characterizations, in order to get a better understanding of the difference in behavior as observed between the gold grid and the platinum paste current collectors. For the Pt-paste, the X-ray analysis revealed the formation of undesirable phases [Figure 5(a)]. To confirm this result, a reactivity test was then performed on pellets prepared by mixing Ca349 and Pt powder and firing at 700 °C for 72 h. Additional peaks corresponding to phases, such as CaPt<sub>2</sub>O<sub>4</sub>, Ca<sub>4</sub>PtO<sub>6</sub>, Ca<sub>3</sub>Co<sub>2</sub>O<sub>6</sub>, and Co<sub>3</sub>O<sub>4</sub>

[Figure 5(b and c)], confirming a chemical reaction between Ca349 and Pt. A study, whose results have never been published before [15], has revealed that the Ca<sub>3</sub>Co<sub>2</sub>O<sub>6</sub> phase, which consists of a one-dimensional structure, has quite poor conducting properties and cathode behavior, as compared to Ca349, with a polarization resistance of 96.2 Ω cm<sup>-1</sup> at 700 °C (Figure 6). The growing contribution observed in the impedance plot could thus be assigned to undesirable phases resulting from the reaction on the surface between Ca349 and the platinum paste.



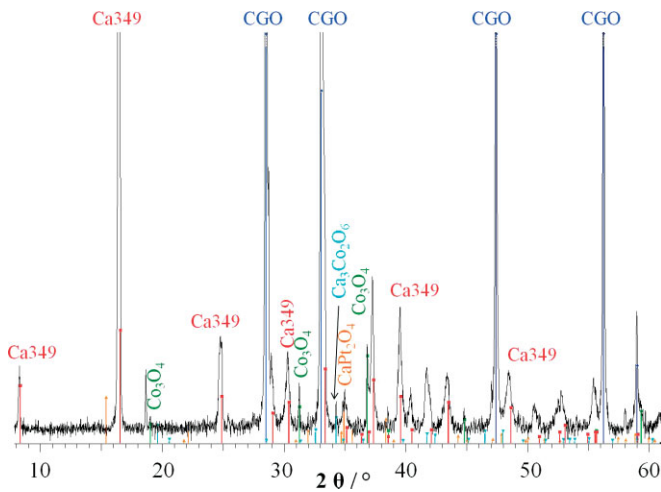


Fig. 7 X-ray diffractograms of CC700<sub>20</sub> after EIS measurements.

In general, for a good CNLS-fit the residuals distribution should be similar in shape as observed for the KK-test [12]. Since the KK-test also indicates the frequency limits that will allow an optimal fit procedure, a significant difference between the residuals plot for the KK-test and the final CNLS-analysis can indicate that the data contains either an additional contribution or that the used equivalent circuit is not appropriate.

Whereas, ZView 3.3a uses a (semi) automatic search for the equivalent circuit with the “best fit” to the data set, EqCwin provides a partial fit and subtraction procedure with which a possible equivalent circuit is built and starting values for the fit parameters are obtained. These are subsequently used for a final overall CNLS-fit of the complete data set. The clear advantage of this procedure is that minor contributions, that are not obvious from visual inspection of the data, are readily detected [7, 12]. Final comparison of the residuals distributions between the KK-test and the CNLS-fit can confirm the viability of the derived equivalent circuit to model the data set. In Figure 8 (a and b) the KK-tests indicate for the data of sample PC800c<sub>10</sub> a perfect KK behavior.

Two possible equivalent circuits can be derived using EqCwin: a series circuit and a nested circuit. A very good match between data set and model function can be observed, as demonstrated in Figure 8(c and d), where the final CLNS-fit of the data measured at 700 °C is presented. The corresponding circuit element values and error estimates are presented in Table 2. The nested arrangement assumes a double layer capacitance between the electrode and the electrolyte, which results in a parallel capacitance to the electrode response. Both circuits have been checked for various temperatures, various compositions (composite 70% Ca<sub>3</sub>Co<sub>4</sub>O<sub>9</sub>–30% CGO, pure Ca<sub>3</sub>Co<sub>4</sub>O<sub>9</sub>), various layer thicknesses, various current collectors (gold grid, gold paste, and platinum paste), various oxygen partial pressure, and leads to good fits of similar quality. The extracted circuits correspond to the minimal number of contributions necessary for a good fit quality. Adding an extra circuit does not automati-

cally improve the fit. Inappropriate additions to the EqCwin will generally result in a shift of the element parameters to either zero or infinity during the fit procedure. Particular focus should be paid on the errors obtained in ZView and EqCwin which are not calculated in the same way, then, the obtained values cannot be compared. The errors in ZView are based on the number of experimental points considered, whereas, the error estimates in EqCwin are based on the assumption that the residual errors can be assumed to represent the parent distribution [8, 12]. This last point requires that the residuals are randomly distributed around the log( $\omega$ ) axis. A systematic deviation from 0 around the log( $\omega$ ) axis invalidates the calculation of the error estimates.

Here, as example, we present Figure 8 and Table 2 the results concerning only the impedances data measured at 700 °C under air atmosphere. The specific resistances associated to a frequency range are of the same order of magnitude, whatever the type of circuit, series or nested. That means, with the chosen notation:  $(R_1)_{\text{series}} = (R_1)_{\text{nested}}$ ;  $(R_2)_{\text{series}} = (R_4)_{\text{nested}}$ ;  $(R_3)_{\text{series}} = (R_2)_{\text{nested}}$ ;  $(R_4)_{\text{series}} = (R_3)_{\text{nested}}$ ; and  $(R_5)_{\text{series}} = (R_5)_{\text{nested}}$ . Both circuits involve the same number of parameters. The series circuit imply successive steps in the cathode reaction, whereas, the nested one, consider one step occurring at the same time as the other ones.

Considering the ZView 3.3a program, an equivalent circuit consisting of a series association of a finite Warburg (W) and (R//CPE) elements is extracted, corroborating the results of previous studies [4]. A comparison between the fitted model and the experimental data is provided in the Supplementary Section S5. The corresponding circuit elements are given Table 2.

The two fit procedures, ZView and EqCwin, lead in the case of PC800c<sub>10</sub> to quite different model circuits. But for a comparison purpose, the series circuits extracted from EqCwin has been applied in ZView (Supplementary data S6). However, a small improvement of the fit is observed because of the higher number of fitted elements. But the additional part of the circuit is associated to a too big error to be considered. By constructing progressively the circuit, using various data in function of the temperature, the first proposed ZView circuit with the corresponding errors is more justified. Moreover, if the nested circuit is applied in ZView, the fit is not stable (Supplementary data S6).

As the series and the nested circuits extracted from EqCwin lead to the same fit quality and as the application of the nested circuit in ZView is unstable, for an easier comparison between the two softwares, the series circuit only will be considered for the rest of the study. Knowing that CCO is a mixed ionic–electronic conductor, we can expect several intermediate mechanisms, involving the surface reaction, the electrode–electrolyte interface diffusion, and the diffusion in the cathode itself. They cannot be clearly identified using the elementary ZView circuit with two (even three) contributions, which provide a too rough description. In that case, the subtraction technique developed in EqCwin leads to a more complex circuit consisting of four contributions corresponding to the best fit quality with the minimal number of contri-



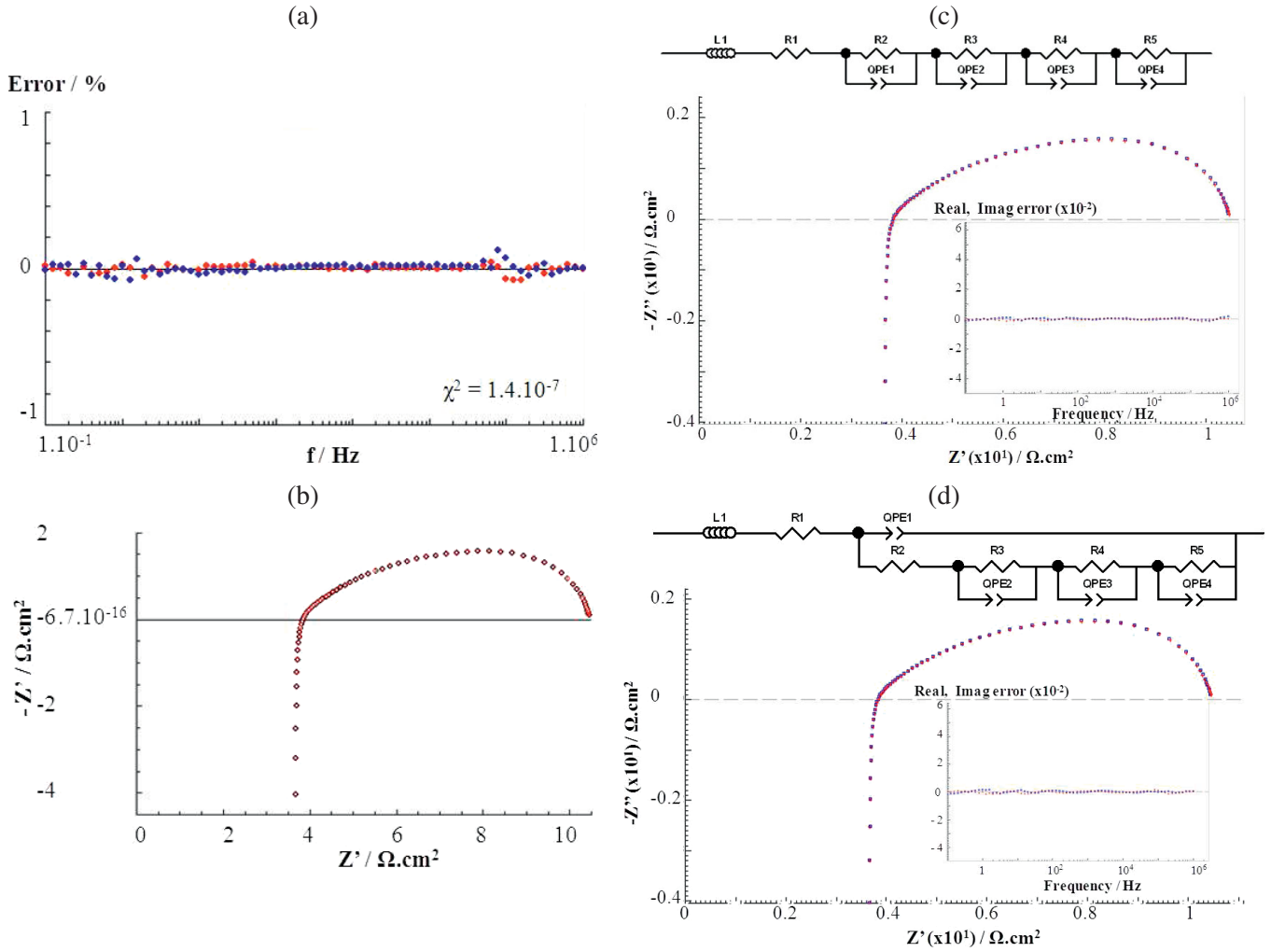


Fig. 8 (a) KK tests for PC800c<sub>10</sub>. The red plot corresponds to the real part differences and the blue plot to the imaginary part differences. (b) Ideal fits possible to get using the considered data set for PC800c<sub>10</sub>. Fit is represented in red and impedance data in black. (c and d) Comparison of the experimental and fitted impedance plots of PC800c<sub>10</sub>, using the subtraction procedure on Equivalent Circuit 1.2 software, considering the series and the nested equivalent circuit, respectively. The corresponding residual plots are reported in insert. Fit are represented in red cross and impedance data in blue square.

Table 2 PC800c<sub>10</sub>: comparison of the fitted circuit elements using ZView 3.3a and Equivalent Circuit 1.2 softwares.

ZView 3.3a		EqCwin 1.2	
Circuit description	Circuit description	Circuit description	Circuit description
$R_1 L_1 W_s (R_2 // CPE_1)$ [5]	$R_1 L_1 W_s (R_2 // CPE_1) (R_3 // CPE_2)$	$L_1 R_1 (R_2 Q_1) (R_3 Q_2) (R_4 Q_3) (R_5 Q_4)$	$L_1 R_1 (Q_1 [R_2 (R_3 Q_2) (R_4 Q_3) (R_5 Q_4)])$
$t = 696$ °C	$t = 696$ °C	$t = 696$ °C	$t = 696$ °C
Circuit elements	Circuit elements	Circuit elements	Circuit elements
$R_1 = 3,557$ Ω (0.1%)	$R_1 = 3,557$ Ω (0.1%)	$L_1 = 6.5 \times 10^{-7}$ Henri (0.1%)	$L_1 = 6.5 \times 10^{-7}$ Henri (0.1%)
$L_1 = 6.5 \times 10^{-7}$ Henri (0.1%)	$L_1 = 6.5 \times 10^{-7}$ Henri (0.1%)	$R_1 = 3.6$ Ω (0.4%)	$R_1 = 3.7$ Ω (0.2%)
$W_s - R = 3.64$ (2%)	$W_s - R = 2.10$ (3%)	$R_2 = 1.7$ Ω (35.2%)	$Q_1 - Y_0 = 2.2 \times 10^{-1}$ mho (104.8%)
$W_s - T = 0.0046$ (5%)	$W_s - T = 0.0018$ (5%)	$Q_1 - n = 9.3 \times 10^{-1}$ (4.1%)	$Q_1 - n = 7.4 \times 10^{-1}$ (10.3%)
$W_s - P = 0.336$ (0.5%)	$W_s - P = 0.309$ (1%)	$R_3 = 6.2$ Ω (79.2%)	$R_2 = 3.1 \times 10^{-1}$ Ω (29.6%)
		$Q_2 - Y_0 = 2.3 \times 10^{-2}$ mho (45.4%)	$Q_2 - Y_0 = 6.9 \times 10^{-3}$ mho (18.9%)
$R_2 = 3.33$ Ω (2%)	$R_2 = 2.9$ Ω (8%)	$Q_2 - n = 4.1 \times 10^{-1}$ (11.1%)	$Q_2 - n = 5.4 \times 10^{-1}$ (4.4%)
$CPE_1 - T = 0.0124$ (2%)	$CPE_1 - T = 0.0071$ (7%)	$R_4 = 2.6$ Ω (76.9%)	$R_4 = 2.2$ Ω (62.6%)
$CPE_1 - P = 0.797$ (1%)	$CPE_1 - P = 0.71$ (2%)	$Q_3 - Y_0 = 5.7 \times 10^{-3}$ mho (17.6%)	$Q_3 - Y_0 = 8.3 \times 10^{-3}$ mho (9.1%)
		$Q_3 - n = 6.0 \times 10^{-1}$ (12.3%)	$Q_3 - n = 7.4 \times 10^{-1}$ (14.5%)
	$R_3 = 1.8$ Ω (11%)	$R_5 = 2.0$ Ω (105.0%)	$R_5 = 1.7$ Ω (25.8%)
	$CPE_2 - T = 0.021$ (7%)	$Q_4 - Y_0 = 9.4 \times 10^{-3}$ mho (18.3%)	$Q_4 - Y_0 = 2.1 \times 10^{-2}$ mho (19.0%)
	$CPE_2 - P = 0.91$ (2%)	$Q_4 - n = 7.8 \times 10^{-1}$ (21.2%)	$Q_4 - n = 9.3 \times 10^{-1}$ (3.6%)
$\chi^2 = 6.3 \times 10^{-5}$	$\chi^2 = 6.3 \times 10^{-6}$	$\chi^2 = 3.6 \times 10^{-7}$	$\chi^2 = 5.5 \times 10^{-7}$

butions, which may provide additional information on the cathode behavior.

To have a better understanding of the current collector and of the layer thickness, the same analysis approach will be applied on selected composite cathodes. We have focused on a cell with a composite Ca349 cathode, measured successively with a gold grid and with platinum paste (cathodes: CC800<sub>5</sub> and CC800Pt<sub>5</sub>) and second cell with a thicker cathode layer (20 μm), measured successively with a gold grid and gold paste (cathodes: CC800<sub>20</sub> and CC800Au<sub>20</sub>). A detailed com-

parison is performed on the CNLS-fits of the impedance data collected at 700 °C.

Using ZView, the fit procedure considers the whole data set and leads to the following series circuit:  $R_1L_1W_s(R_2//CPE_1)$  [4] and  $R_1L_1W_s(R_2//CPE_1)(R_3//CPE_2)$ . In the case of Pt paste as current collector the contribution ( $R_3//CPE_2$ ) obtained in the low frequency range is widely increased, compared to Au grid collector. No particular information of the cathode behavior can be extracted. The ZView and CNLS-fit results are provided in Table 3 and Figure 9. One

Table 3 CC800<sub>5</sub>, CC800Pt<sub>5</sub>, CC800<sub>20</sub>, and CC800Au<sub>20</sub>: fitted circuit elements using ZView 3.3a software.

Fit results 700 °C–ZView 3.3a							
	CC800 <sub>5</sub> [5] and this work		CC800Pt <sub>5</sub> [5]		CC800 <sub>20</sub>	CC800Au <sub>20</sub>	
R <sub>1</sub>	5.3 Ω (0.08%)	5.3 Ω (0.05%)	3.06 Ω (0.6%)	4.2 Ω (0.2%)	4.2 Ω (0.3%)	2.8 Ω (0.3%)	2.8 Ω (0.3%)
L <sub>1</sub>	6.5 × 10 <sup>-7</sup>	6.5 × 10 <sup>-6</sup>	5.9 × 10 <sup>-7</sup>	1.5 × 10 <sup>-6</sup>	1.5 × 10 <sup>-6</sup>	1.6 × 10 <sup>-6</sup>	1.6 × 10 <sup>-6</sup>
	Henri (0.2%)	Henri (0.06%)	Henri (0.8%)	Henri (0.4%)	Henri (0.4%)	Henri (0.4%)	Henri (0.4%)
WR	3.31c (3%)	4.7 (1.5%)	1.9 (25%)	1.3 (8%)	0.97 (69%)	0.9 (50%)	0.9 (47%)
WT	0.0052 (6%)	0.018 (9%)	1.1 × 10 <sup>-4</sup> (14%)	0.006 (24%)	0.009 (40%)	0.003 (24%)	0.008 (35%)
WP	0.4 (0.7%)	0.33 (0.5%)	0.42 (6%)	0.3 (2%)	0.3 (20%)	0.3 (2%)	0.3 (14%)
R <sub>2</sub>	2.67 Ω (4%)	0.68 Ω (15%)	6.3 Ω (11%)	0.4 Ω (28%)	0.22 Ω (72%)	0.6 Ω (14%)	0.4 Ω (40%)
CPE <sub>1-T</sub>	0.017 (5%)	0.064 (9%)	0.0074 (10%)	0.01 (15%)	0.19 (55%)	0.06 (7%)	0.1 (31%)
CPE <sub>1-P</sub>	0.73 (2%)	0.96 (3%)	0.48 (8%)	0.7 (6%)	0.85 (12%)	0.8 (4%)	0.8 (7%)
R <sub>3</sub>		0.49 Ω (18%)	5.6 Ω (6%)		0.38 Ω (130%)		0.35 Ω (80%)
CPE <sub>2-T</sub>		0.006 (19%)	0.103 (5%)		0.03 (83%)		0.02 (60%)
CPE <sub>2-P</sub>		0.75 (5%)	0.830 (3%)		0.5 (32%)		0.5 (20%)
χ <sup>2</sup>	4.3 × 10 <sup>-5</sup>	7.3 × 10 <sup>-6</sup>	2 × 10 <sup>-4</sup>	4.8 × 10 <sup>-5</sup>	2.5 × 10 <sup>-5</sup>	1 × 10 <sup>-4</sup>	3 × 10 <sup>-5</sup>

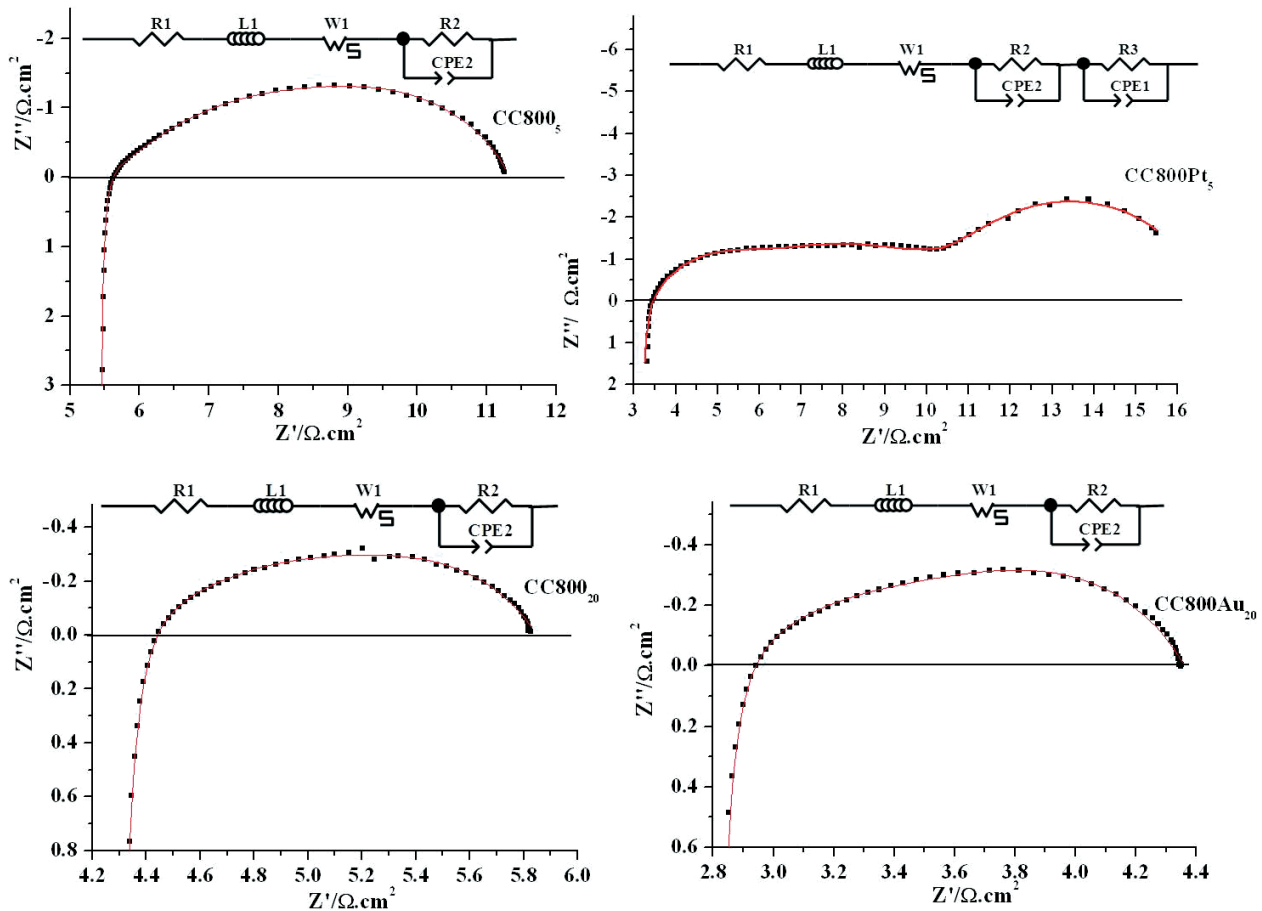


Fig. 9 Experimental impedance plots and the corresponding fits using ZView 3.3a for CC800<sub>5</sub>, CC800Pt<sub>5</sub>, CC800<sub>20</sub>, and CC800Au<sub>20</sub>.

must notice, in case of cells measured with the gold paste or gold grid as current collector, that the last part of the circuit ( $R_3//CPE_2$ ) is not necessarily justified, the associated errors being high for a slightly improved  $R_p$  value. The equivalent circuit evidenced in ZView is in good agreement with the circuits reported in refs. [4, 5] for the pure and composite compounds.

For the subtraction procedure, the quality of the data is first checked using the KK test. The data are of quite good quality, except for CC800Pt<sub>5</sub>, where a larger noise contribution is observed in the low frequency region. The KK-test residuals and CNLS-fit results are presented in Figures S7 and S8 of the Supplementary Data Section. The circuits extracted pre-

viously on the pure compound, measured with a gold grid as current collectors, were applied to the composite compounds studied in this part. For a better comparison with ZView fits, the series equivalent circuit will be considered, as it is equal to the other one with respect to the fit quality. The series equivalent circuit  $L_1R_1(R_2Q_1)(R_3Q_2)(R_4Q_3)(R_5Q_4)$  describes properly CC800<sub>5</sub>, CC800<sub>20</sub>, and CC800Au<sub>20</sub>. One can notice that the same circuit can be used for CC800Pt<sub>5</sub>. The fit results are presented in Table 4 and the corresponding CNLS-fits compared to the experimental data in Figure 10. The first point to notice is that the pure and the composite compounds show the same behavior, as evidenced by the same equivalent circuits. This means that the same physical phenomena are

Table 4. CC800<sub>5</sub>, CC800Pt<sub>5</sub>, CC800<sub>20</sub>, and CC800Au<sub>20</sub>: fitted circuit elements using Equivalent Circuit 1.2 software.

CC800 <sub>5</sub> $t = 714$ °C	CC800Pt <sub>5</sub> $t = 701$ °C	CC800 <sub>20</sub> $t = 701$ °C	CC800Au <sub>20</sub> $t = 702$ °C
$L_1R_1(R_2Q_1)(R_3Q_2)(R_4Q_3)(R_5Q_4)$	$L_1R_1(R_2Q_1)(R_3Q_2)(R_4Q_3)(R_5Q_4)$	$L_1R_1(R_2Q_1)(R_3Q_2)(R_4Q_3)(R_5Q_4)$	$L_1R_1(R_2Q_1)(R_3Q_2)(R_4Q_3)(R_5Q_4)$
$L_1 = 6.5 \times 10^{-7}$ Henri (0.1%)	$L_1 = 5.6 \times 10^{-7}$ Henri (0.8%)	$L_1 = 1.5 \times 10^{-6}$ Henri (0.9%)	$L_1 = 1.6 \times 10^{-6}$ Henri (0.4%)
$R_1 = 5.4$ Ω (0.2%)	$R_1 = 3.2$ Ω (0.7%)	$R_1 = 4.3$ Ω (0.6%)	$R_1 = 2.8$ Ω (0.8%)
$R_2 = 2.2$ Ω (80.3%)	$R_2 = 1.9$ Ω (79%)	$R_2 = 5.9 \times 10^{-1}$ Ω (101.4%)	$R_2 = 5.1 \times 10^{-1}$ Ω (137.4%)
$Q_1 - Y_0 = 1.0 \times 10^{-2}$ mho (25.9%)	$Q_1 - Y_0 = 2.9 \times 10^{-4}$ mho (29.8%)	$Q_1 - Y_0 = 1.4 \times 10^{-2}$ mho (105.1%)	$Q_1 - Y_0 = 1.7 \times 10^{-2}$ mho (61.8%)
$Q_1 - n = 7.7 \times 10^{-1}$ (16.0%)	$Q_1 - n = 7.2 \times 10^{-1}$ (11.3%)	$Q_1 - n = 5.8 \times 10^{-1}$ (32.7%)	$Q_1 - n = 6.6 \times 10^{-1}$ (31.3%)
$R_3 = 0.7$ Ω (70.1%)	$R_3 = 3.0$ Ω (85.4%)	$R_3 = 2.6 \times 10^{-1}$ Ω (64.0%)	$R_3 = 2.2 \times 10^{-1}$ Ω (71.3%)
$Q_2 - Y_0 = 1.8 \times 10^{-2}$ mho (30.1%)	$Q_2 - Y_0 = 2.3 \times 10^{-3}$ mho (50.2%)	$Q_2 - Y_0 = 2.0 \times 10^{-1}$ mho (59.4%)	$Q_2 - Y_0 = 2.1 \times 10^{-1}$ mho (67.7%)
$Q_2 - n = 4.3 \times 10^{-1}$ (7.4%)	$Q_2 - n = 6.3 \times 10^{-1}$ (29.5%)	$Q_2 - n = 8.4 \times 10^{-1}$ (10.3%)	$Q_2 - n = 9.0 \times 10^{-1}$ (8.3%)
$R_4 = 2.2$ Ω (82.0%)	$R_4 = 2.6$ Ω (42.5%)	$R_4 = 5.6 \times 10^{-1}$ Ω (100.5%)	$R_4 = 4.7 \times 10^{-1}$ Ω (122.7%)
$Q_3 - Y_0 = 6.2 \times 10^{-3}$ mho (20.8%)	$Q_3 - Y_0 = 1.1 \times 10^{-2}$ mho (29.7%)	$Q_3 - Y_0 = 2.5 \times 10^{-1}$ mho (39.9%)	$Q_3 - Y_0 = 3.3 \times 10^{-2}$ mho (31.3%)
$Q_3 - n = 6.2 \times 10^{-1}$ (14.3%)	$Q_3 - n = 7.1 \times 10^{-1}$ (8.6%)	$Q_3 - n = 7.4 \times 10^{-1}$ (24.5%)	$Q_3 - n = 8.0 \times 10^{-1}$ (25.8%)
$R_5 = 7.8 \times 10^{-1}$ Ω (42.1%)	$R_5 = 5.9$ Ω (2.0%)	$R_5 = 1.3 \times 10^{-1}$ Ω (145.2%)	$R_5 = 4.0 \times 10^{-1}$ Ω (77.7%)
$Q_4 - Y_0 = 6.8 \times 10^{-2}$ mho (36.5%)	$Q_4 - Y_0 = 9.4 \times 10^{-2}$ mho (2.1%)	$Q_4 - Y_0 = 2.3 \times 10^{-3}$ mho (237.3%)	$Q_4 - Y_0 = 1.5 \times 10^{-2}$ mho (88.8%)
$Q_4 - n = 9.4 \times 10^{-1}$ (5.7%)	$Q_4 - n = 8.3 \times 10^{-1}$ (1.1%)	$Q_4 - n = 6.8 \times 10^{-1}$ (40.9%)	$Q_4 - n = 4.9 \times 10^{-1}$ (19.2%)
$\chi^2 = 2.5 \times 10^{-7}$	$\chi^2 = 3.7 \times 10^{-6}$	$\chi^2 = 6.1 \times 10^{-7}$	$\chi^2 = 2.7 \times 10^{-7}$

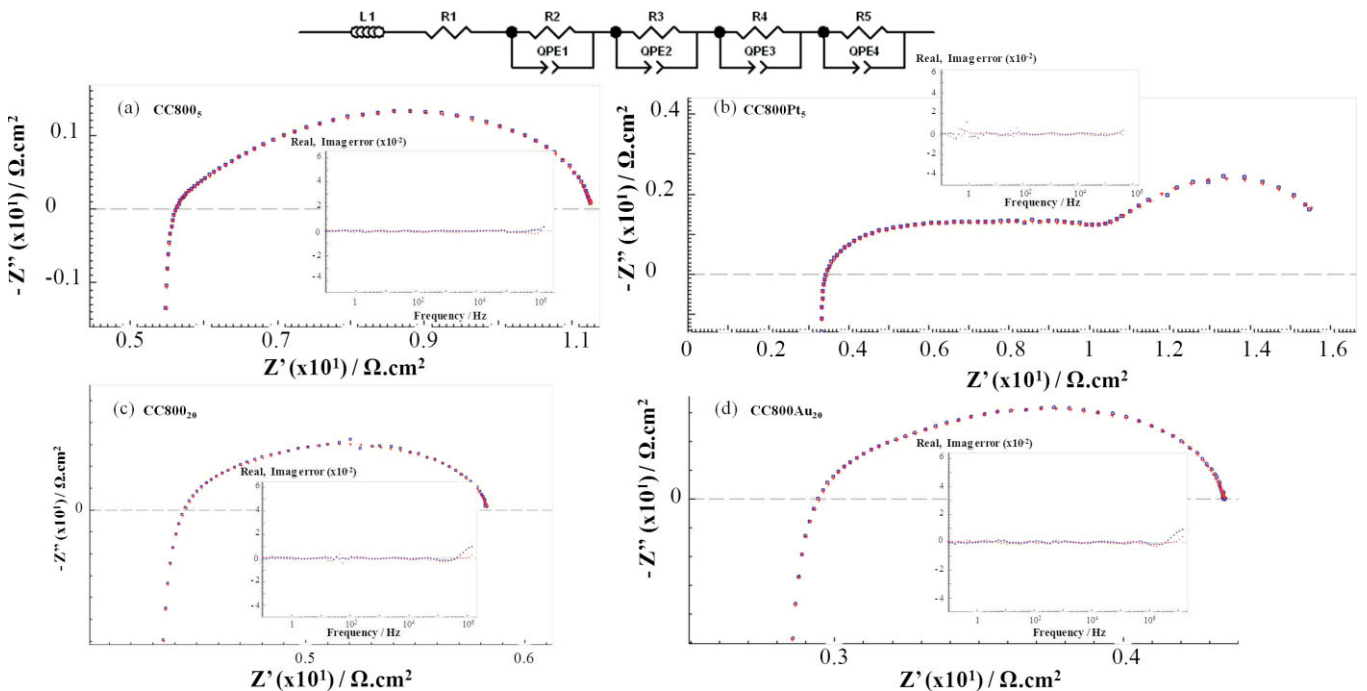


Fig. 10 Experimental impedance plots and the corresponding fits using EqCwin 1.2 for (a) CC800<sub>5</sub>, (b) CC800Pt<sub>5</sub>, (c) CC800<sub>20</sub>, and (d) CC800Au<sub>20</sub>. The corresponding residual plots are in insert.

involved independently of the composition of the cathode: pure Ca349 or composite 70 wt.% Ca349–30 wt.% CGO.

In the following sections, the focus is on the subtraction procedures using EqCwin, considering the series equivalent circuit. Some large errors can be noticed. But they are just a consequence of the cross-correlation between parameters. From a general point of view, the errors in the ZView fit appear to be lower, but this is due to the systematic deviation in the residual plots. Knowing that, a correlation between the circuit contributions and physical phenomena has been suggested.

#### Behavior of CC800<sub>5</sub> Versus CC800Pt<sub>5</sub>

As presented above, a comparison of the same CC800 cathodes, either with gold grid or with platinum paste current collectors, reveals that two different equivalent circuits: a series and a parallel circuit, could be considered.

As frequency decreases, the resistances appear in the order:  $R_1$ ,  $R_3$ ,  $R_4$ ,  $R_2$ , and  $R_5$ . The resistance parallel to a capacitor chosen to describe the low frequency contribution is related to surface phenomena associated either with the platinum paste or the degradation phases. The high and medium frequency semicircles correspond to the electrochemical behavior associated with the combination of Ca349 and the degradation phases, which constitutes a new cathode. This changed cathode composition leads to quite different electrochemical properties. One can notice that  $R_1$ ,  $R_2$ , and  $R_4$  are of the same order of magnitude, whereas, using platinum paste as current collector leads to an increase of  $R_3$  and  $R_5$ .

#### Behavior of CC800<sub>20</sub> Versus CC800Au<sub>20</sub>

CC800<sub>20</sub> and CC800Au<sub>20</sub> cathodes responses are both described by a series equivalent circuit. The characteristic resistances appear, with decreasing frequency, in the order  $R_1$ ,  $R_3$ ,  $R_4$ ,  $R_2$ , and  $R_5$ . Special attention paid to the fitted values of the circuit elements (Table 4) reveals that the same order of magnitude is observed for both cathodes. This confirms that the same electrochemical reaction applies when using gold paste or gold grid current collectors.

#### Behavior of CC800<sub>5</sub> Versus CC800<sub>20</sub>

These two samples differ in their layer thickness. CC800<sub>5</sub> and CC800<sub>20</sub> have, respectively, a thickness of 5 and 20  $\mu\text{m}$ . Assuming that each contribution in the equivalent circuit can be associated with different steps in the overall electrochemical cathode reaction, one could assign  $R_3$  and  $R_4$  to diffusion phenomena in the cathode layer according to their frequency location on the plot in the 13–10 000 Hz range, approximately, corresponding to the “C arc” mentioned in the ref. [16]. Similarly  $R_5$  can be assigned to surface phenomena and  $R_2$  to the electrode–electrolyte interface impedance. For both samples, the  $R_5$  values and associated time constants are of the same order of magnitude. For  $R_2$ , differences are evidenced for R values, but the associated time constants are

similar. For  $R_3$  and  $R_4$ , differences are noticed for R values and time constant. It seems to indicate that the surface and interface phenomena are not affected by the thickness effect. However, the diffusion phenomenon is affected by the thickness effect. The same physical phenomenon is involved and the thickness affects highly the resistances values. The thick layer shows the lowest polarization resistance. This indicates the importance of the mixed conduction properties of the material and the increased triple phase boundary length which is essential for the oxygen reduction reaction.

## 4 Conclusion

Ca<sub>3</sub>Co<sub>4</sub>O<sub>9- $\delta$</sub>  (Ca349) is a mixed ionic, electronic conductor with interesting electrochemical properties, which makes it a good candidate cathode for application in a SOFC. Continued investigations are underway to improve the properties and to understand the electrochemical behavior of this material. Complex mechanisms are involved at the cathode which are much more complicated in case of the composite cathode/electrolyte. EIS is a key technique to describe the cathode behavior. However, special attention should be paid to the choice of the current collector, which depends on the composition under study. This study, focused on Ca349, revealed that in this case the best current collector is a gold grid. The commonly used platinum paste or grid is here inappropriate as current collector for the SOFC cathode. Reactions between Ca349 and platinum lead to the formation of several undesirable phases: CaPt<sub>2</sub>O<sub>4</sub>, Ca<sub>4</sub>PtO<sub>6</sub>, Ca<sub>3</sub>Co<sub>2</sub>O<sub>6</sub>, and Co<sub>3</sub>O<sub>4</sub>. With platinum paste as current collector, the electrode impedance clearly shows two contributions, whereas, with a gold grid current collector only one contribution is observed. Two fit procedures, ZView 3.3a and EqCwin v1.2 were applied for the impedance data analysis. The subtraction procedure provided in EqCwin yields more detailed information on the equivalent circuits than ZView. The CNLS-analysis has made it possible to study the effect of current collector and layer thickness, as part of the study of electrode materials. To confirm the correlation between the circuit elements and the physical phenomena, further electrochemical studies considering various electrode compositions and microstructural properties will be performed under various conditions (temperature, atmosphere, and current). A perspective of the work could be also to describe the actual electrode structure with finite element modeling, as reported by Kornely et al. [17].

## Acknowledgements

The PHC Alliance exchange programme is acknowledged for funding the collaboration with Prof. Irvine’s group, at the University of St Andrews. We thank the group for performing screen-printing depositions. K. Nagasawa and H. Nakatsugawa are thanked for initiating the work on the Ca349 material. Nicolas Preux is acknowledged for the results on Ca<sub>3</sub>Co<sub>2</sub>O<sub>6</sub>, which are part of his PhD.

## Supplementary Data Section

Ca349 and LSCF refer to  $\text{Ca}_3\text{Co}_4\text{O}_{9+\delta}$  and  $\text{La}_{0.6}\text{Sr}_{0.4}\text{Co}_{0.8}\text{Fe}_{0.2}\text{O}_3$ , respectively. EIS refer to electrochemical impedance spectroscopy.

S1 Legend of the abbreviations considered.

Composition	Treatment $t$ / °C	Support	Current collector	Thickness / $\mu\text{m}$	Name	Reference
Pure $\text{Ca}_3\text{Co}_4\text{O}_{9+\delta}$	700 °C	Dense CGO	Au grid	~40	PC700 <sub>40</sub>	[4]
Composite 70 wt.% $\text{Ca}_3\text{Co}_4\text{O}_{9+\delta}$ -30 wt.% CGO	700 °C	Dense CGO	Au grid	~15	CC700 <sub>15</sub>	[4]
Pure $\text{Ca}_3\text{Co}_4\text{O}_{9+\delta}$ + 20 wt.% cellulose	800 °C	Dense CGO	Au grid	5-10	PC800c <sub>10</sub>	[5]
Pure $\text{Ca}_3\text{Co}_4\text{O}_{9+\delta}$ + 20 wt.% cellulose	900 °C	Dense CGO	Pt paste	~10	PC900cPt <sub>10</sub>	[5]
Composite 70 wt.% $\text{Ca}_3\text{Co}_4\text{O}_{9+\delta}$ -30 wt.% CGO	800 °C	Dense CGO	Au grid	~5	CC800 <sub>5</sub>	[5]
Composite 70 wt.% $\text{Ca}_3\text{Co}_4\text{O}_{9+\delta}$ -30 wt.% CGO	800 °C	Dense CGO	Pt paste	~5	CC800Pt <sub>5</sub>	[5]
Composite 70 wt.% $\text{Ca}_3\text{Co}_4\text{O}_{9+\delta}$ -30 wt.% CGO	800 °C	Dense CGO	Au grid	~20	CC800 <sub>20</sub>	[5]
Composite 70 wt.% $\text{Ca}_3\text{Co}_4\text{O}_{9+\delta}$ -30 wt.% CGO	800 °C	Dense CGO	Au paste	~20	CC800Au <sub>20</sub>	This work
Composite 70 wt.% $\text{Ca}_3\text{Co}_4\text{O}_{9+\delta}$ -30 wt.% CGO	700 °C	Dense CGO	Pt grid	~20	CC700 <sub>20</sub>	This work

S2 Cell characteristics.

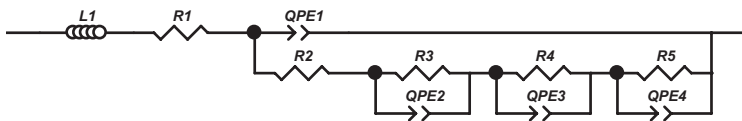
$R_1 // CPE_1$ :



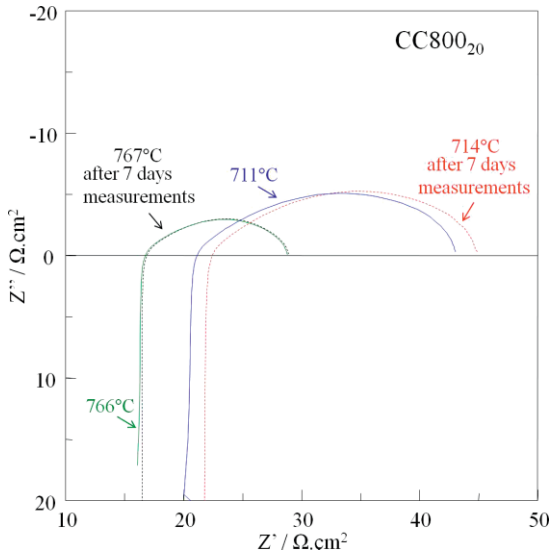
$L_1 R_1 (R_2 Q_1) (R_3 Q_2) (R_4 Q_3) (R_5 Q_4)$ :



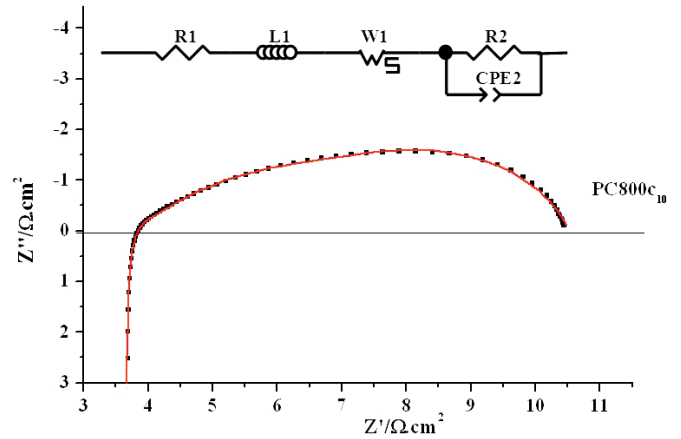
$L_1 R_1 (Q_1 [R_2 (R_3 Q_2) (R_4 Q_3) (R_5 Q_4)])$ :



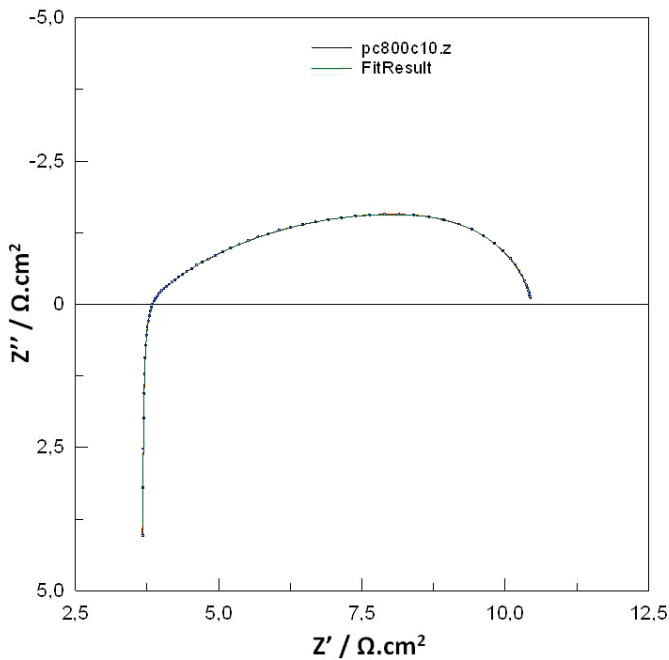
S3 Equivalent circuits symbols.



S4 Evolution of gold grid cell CC800Au<sub>20</sub>, before and after 7 days measurements.

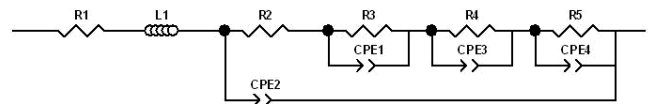


S5 Comparison of the experimental and fitted impedance plots of PC800c<sub>10</sub> using ZView 3.3a software. Fit are represented in red line and impedance data in black square.



Element	Freedom	Value	Error	Error %
R1	Free(±)	3,602	0,013394	0,37185
L1	Free(±)	6,5099E-07	5,3044E-10	0,081482
R2	Free(+)	1,996	2,0808	104,25
CPE1-T	Free(±)	0,0094527	0,0017088	18,077
CPE1-P	Free(±)	0,77953	0,16412	21,054
R3	Free(±)	2,58	1,9609	76,004
CPE2-T	Free(±)	0,0057415	0,00099616	17,35
CPE2-P	Free(±)	0,60446	0,073552	12,168
R4	Free(±)	0,62468	0,48923	78,317
CPE3-T	Free(±)	0,0226	0,010188	45,08
CPE3-P	Free(±)	0,40623	0,044433	10,938
R5	Free(±)	1,696	0,5913	34,864
CPE4-T	Free(±)	0,023453	0,0070389	30,013
CPE4-P	Free(±)	0,92759	0,037581	4,0515

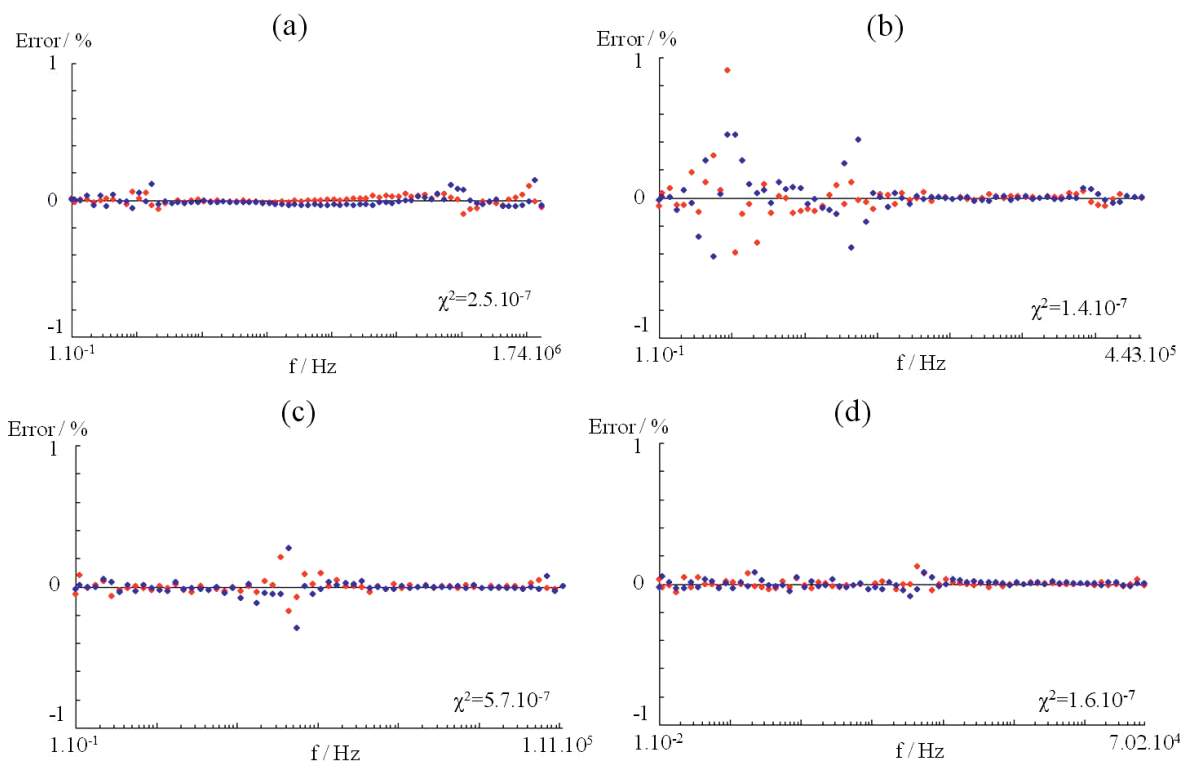
Chi-Squared: 3,9053E-06  
Weighted Sum of Squares: 0,00049988



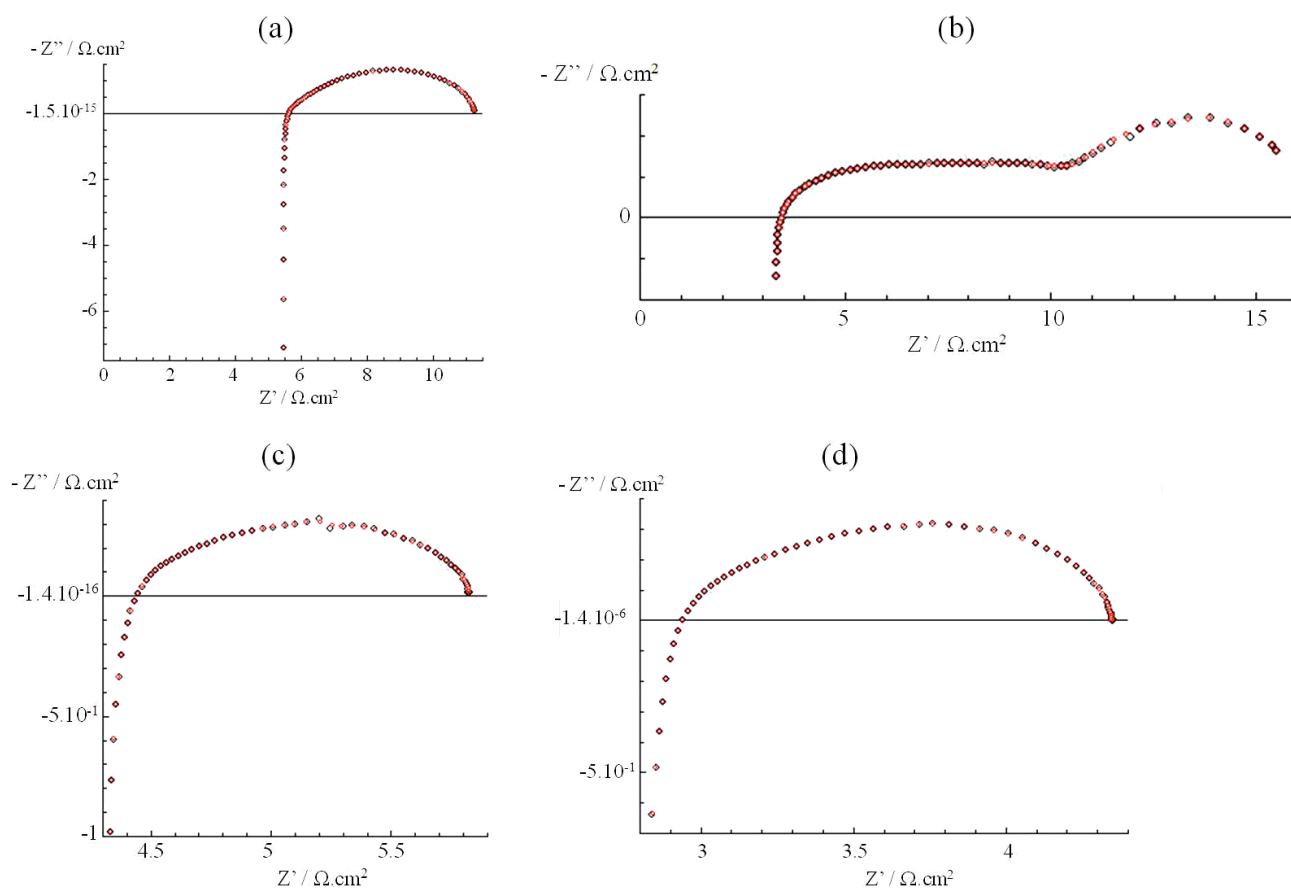
Element	Freedom	Value	Error	Error %
R1	Free(±)	3,655	0,0082636	0,22609
L1	Free(±)	6,4854E-07	6,832E-10	0,10534
R2	Free(+)	0,31144	0,091248	29,299
R3	Free(±)	2,605	1,0317	39,605
CPE1-T	Free(±)	0,0069382	0,001295	18,665
CPE1-P	Free(±)	0,53822	0,023215	4,3133
R4	Free(±)	2,215	1,3745	62,054
CPE3-T	Free(±)	0,0082564	0,00074475	9,0203
CPE3-P	Free(±)	0,744	0,10716	14,403
R5	Free(±)	1,724	0,44024	25,536
CPE4-T	Free(±)	0,021274	0,0040123	18,86
CPE4-P	Free(±)	0,92839	0,03324	3,5804
CPE2-T	Free(±)	0,00021776	0,0002262	103,88
CPE2-P	Free(±)	0,7383	0,075089	10,171

Chi-Squared: 5,953E-06  
Weighted Sum of Squares: 0,00076199

S6 Test in ZView of the series and the nested equivalent circuits extracted using EqCwin.



S7 Kramers–Kronig tests for (a) CC800<sub>5</sub>, (b) CC800Pt<sub>5</sub>, (c) CC800<sub>20</sub>, and (d) CC800Au<sub>20</sub>. The red plot corresponds to the real part differences and the blue plot to the imaginary part differences.



S8 Ideal fits possible to get using the considered data set of (a) CC800<sub>5</sub>, (b) CC800Pt<sub>5</sub>, (c) CC800<sub>20</sub>, and (d) CC800Au<sub>20</sub>.

## References

- [1] S. B. Adler, *Chem. Rev.* **2004**, *104*, 4791.
- [2] H. S. Isaacs, L. J. Olmer, E. J. L. Schouler, C. Y. Yang, *Solid State Ionics* **1981**, *3–4*, 503.
- [3] J. Mizusaki, K. Amano, S. Yamauchi, K. Fueki, *Solid State Ionics* **1987**, *22*, 313.
- [4] K. Nagasawa, S. Daviero-Minaud, N. Preux, A. Rolle, P. Roussel, H. Nakatsugawa, O. Mentré, *Chem. Mater.* **2009**, *21*, 4738.
- [5] A. Rolle, S. Boulfrad, K. Nagasawa, H. Nakatsugawa, O. Mentré, J. Irvine, S. Daviero-Minaud, *J. Power Sources* **2011**, *196*, 7328.
- [6] D. Johnson, Z View version 3.3a, copyright **1990–2011**, Schribner Associates, Inc.
- [7] B. A. Boukamp, *Solid State Ionics* **1986**, *18–19*, 136.
- [8] B. A. Boukamp, *Solid State Ionics* **1986**, *20*, 31.
- [9] B. A. Boukamp, Equivalent Circuit (version 1.2), copyright **1985–2009**, University of Twente/WisseQ.
- [10] E. Capoen, M. C. Steil, G. Nowogrocki, M. Malys, C. Pirovano, A. Löfberg, E. Bordes-Richard, J. C. Boivin, G. Mairesse, R. N. Vannier, *Solid State Ionics* **2006**, *177*, 483.
- [11] B. A. Boukamp, *J. Electrochem. Soc.* **1995**, *142 (6)*, 1885.
- [12] B. A. Boukamp, *Solid State Ionics* **2004**, *169 (1–4)*, 65.
- [13] Y. H. Lin, C. W. Nan, Y. Liu, J. Li, T. Mizokawa, Z. Shen, *J. Am. Ceram. Soc.* **2007**, *90*, 132.
- [14] J. Sunarso, S. Baumann, J. M. Serra, W. A. Meulenber, S. Liu, Y. S. Lin, J. C. Diniz da Costa, *J. Membr. Sci.* **2008**, *320*, 13.
- [15] N. Preux, PhD, UST – Lille 1, “A la Recherche de Nouveaux Matériaux D’électrolyte et de Cathode Pour SOFC : Weberite et Cobaltite”, **2010**.
- [16] M. J. Jorgensen, M. Mogensen, *J. Electrochem. Soc.* **2001**, *148 (5)*, A433.
- [17] M. Kornely, A. Leonide, A. Weber, E. Ivers-Tiffée, *J. Power Sources* **2011**, *196*, 7209.